2018-08

Performance of non-uniform tidal turbine arrays in uniform flow

Bonar, PAJ

10.1007/s40722-018-0118-x
Journal of Ocean Engineering and Marine Energy
Springer Science and Business Media LLC

Journal of Ocean Engineering and Marine Energy manuscript No.
(will be inserted by the editor)

Performance of non-uniform tidal turbine arrays in uniform flow

Paul A. J. Bonar[1,*] · **Thomas A. A. Adcock**[2] ·
Vengatesan Venugopal[1] · **Alistair G. L. Borthwick**[1]

Received: date / Accepted: date

Abstract Theoretical models suggest that in order to maximise their collective power output, tidal turbines should be arranged in a single cross-stream row and optimally spaced to exploit local blockage effects. However, because it is assumed that the turbines within these arrays are identical, such models do not consider the possibility of enhanced power production through the exploitation of spanwise variations in local blockage and resistance. In this paper, we use depth-averaged numerical simulations to investigate whether the performance of a tidal turbine array can be further enhanced by varying solely the local blockage, solely the local resistance, or both local blockage and resistance together, across the array width. Our results suggest that for an initially uniform flow field, the optimal tidal turbine array is also uniform, that is to say that it comprises turbines of equal size, spacing, and resistance. This finding is encouraging because it is more cost-effective and much simpler to design each turbine to be the same and to operate in the same way. Together with earlier findings, these results also suggest a more general, and perhaps unsurprising, conclusion that tidal turbine arrays perform best when designed to match site-specific natural flow conditions.

Keywords Tidal stream power · Tidal turbine array · Shallow water equations · Actuator disc · Non-uniform

[1] School of Engineering, University of Edinburgh, Mayfield Road, Edinburgh EH9 3FB, UK
[2] Department of Engineering Science, University of Oxford, Parks Road, Oxford OX1 3PJ, UK
[*] Corresponding author: p.bonar@ed.ac.uk

1 Introduction

In designing a wind or tidal turbine, one of the key challenges is to understand how the performance of the turbine is defined by its interactions with the flow field. This problem is complicated by the need to describe fluid-structure interactions over multiple length scales; a task which becomes exceedingly complex for turbines within large arrays (Adcock et al., 2015; Vennell et al., 2015). One way to approach this problem is to use a simple theoretical model to analyse the performance of an idealised turbine in an idealised flow field. The simplest of these models is actuator disc theory, which approximates the spinning turbine rotor as a porous disc of uniform resistance (Burton et al., 2001). Simplifying the turbine structure in this way eliminates the need to resolve flow features at smaller scales, and allows arguments of mass, momentum, and energy to describe how factors such as the geometric blockage ratio and resistance of the turbine affect its performance.

One of the earliest applications of actuator disc theory produced what is commonly termed the Betz limit; a well-known theoretical result which establishes that a wind turbine can extract no more than $\sim$59.3% of the kinetic energy of the air which would pass through the swept area in the absence of the turbine (Betz, 1920; Joukowsky, 1920; Okulov et al., 2012). Despite the simplifications involved in its development, the Betz limit has proven a useful benchmark for wind turbine performance and has inspired numerous extensions to the classical turbine model. In recent years, actuator disc theory has provided valuable insights into the performance of tidal stream turbines, having been extended to approximate more closely the flow conditions that such turbines experience (Garrett & Cummins, 2007; Whelan et al., 2009; Houlsby et al., 2008; Vennell, 2010; Draper et al., 2016) and to analyse their performance when placed in different arrangements (Nishino & Willden, 2012, 2013; Vogel et al., 2016; Draper et al., 2014a,b).

Vennell (2010) has shown that in order to maximise their collective power output, tidal turbines should be placed side-by-side to create a single cross-stream row. By maximising the global blockage ratio, which is defined as the ratio of array swept area to channel cross-sectional area, this arrangement allows the turbines not only to extract more power (Garrett & Cummins, 2007) but to do so more efficiently, with less power lost in wake mix-

ing (Draper et al., 2010). By making a number of additional assumptions, Nishino & Willden (2012, 2013) and Vogel et al. (2016) have shown that the performance of a cross-stream row can be further enhanced by adjusting the lateral spacing between the turbines to optimise the local blockage ratio, which is defined as the ratio of turbine swept area to local flow cross-sectional area. Further analysis by Draper et al. (2014a,b) suggests that a single, carefully spaced, cross-stream row is in fact the optimal arrangement for tidal turbines, ensuring both a higher power output per turbine and approximately equal distributions of thrust and power among the turbines. The two-scale actuator disc model of Nishino & Willden (2012) appears, therefore, to provide the simplest description of an optimal tidal turbine arrangement. However, because the two-scale model assumes that each turbine within the array is identical and that the depth of the idealised channel is uniform across its width, it does not consider the possibility that more power could be produced by exploiting the spanwise variations in local blockage and resistance which may naturally arise in practice.

In this paper, numerical simulations are used to investigate whether the performance of a tidal turbine array can be further enhanced by exploiting such variations. The combined array and channel model developed by Bonar (2017) is first used to simulate steady, uniform, and depth-averaged flow through an idealised channel with low background roughness. A sub-grid-scale actuator disc model is used to introduce an array of global blockage 0.1 and the turbines are arranged to achieve near-optimal uniform local blockage and resistance profiles. Non-uniform profiles are then used to investigate whether the performance of the array can be further enhanced by varying solely the local blockage, solely the local resistance, or both local blockage and resistance together, across the array width. This analysis extends the works of Hunter et al. (2015) and Adcock (2015) to consider the effects of spanwise variations in local blockage as well as local resistance, and to measure array performance in terms of both the collective power output of the turbines and their global power coefficient. The analysis also complements the work of Draper et al. (2016) by examining the performance of a turbine array idealised by a non-uniform local resistance in a uniform flow field, as compared to that of a turbine represented by a uniform local resistance in a non-uniform flow field.

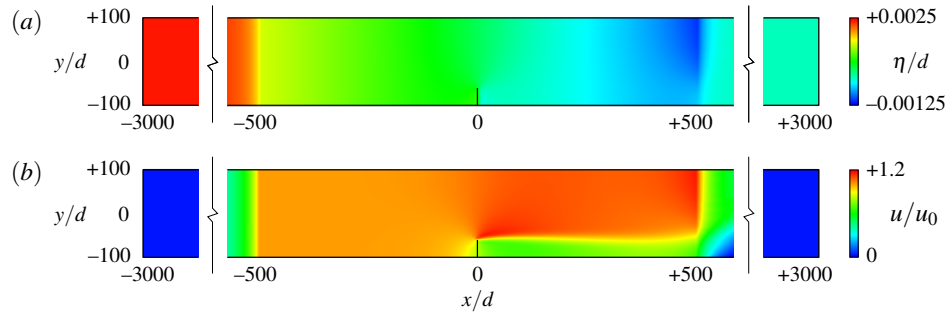

Fig. 1: (Colour online.) Plan views of the model domain showing (near) steady-state contours of: (a) surface elevation $\eta(x,y)$ normalised by channel still water depth d, and; (b) depth-averaged velocity magnitude $u(x,y)$ normalised by unexploited channel velocity u_0. A steady current is driven from left to right by a fixed head difference ζ and the turbine array is extended inward from one side of the channel.

2 Model

Bonar (2017) has developed an idealised numerical model to explore the potential for local blockage effects to enhance the performance of turbines in tidal channels. In this study, the same model is used to analyse the performance of non-uniform tidal turbine arrays in uniform flow. The main features of the model are described as follows.

2.1 Channel-scale flow

Channel-scale flow is simulated by using the open-source hydrodynamic model ADCIRC to solve the depth-averaged shallow water equations by means of a discontinuous Galerkin (DG) finite element scheme (Kubatko et al., 2006, 2009). As illustrated in Fig. 1, the domain of interest is an idealised channel of depth 20 m, width 4 km, and length 20 km. The channel walls are set to allow tangential slip and a steady current is produced by establishing a fixed head difference ζ between the two ocean boundaries, which are placed in deep water (in this case, in water 1 km deep) and positioned far upstream and downstream of the channel (at distances of 50 km) in order to minimise reflections (Adcock, 2015). The contours in Fig. 1a describe a typical variation in free surface elevation, as flow is driven from the upstream ocean boundary at $x/d = -3000$, through the central channel located between $x/d = -500$ and $x/d = +500$ (where the depth drops slightly below the still water level),

and toward the downstream ocean boundary at $x/d = +3000$. The contours in Fig. 1*b* show the corresponding variation in depth-averaged velocity magnitude, with continuity ensuring that velocities are highest in the shallow central channel and practically negligible at the ocean boundaries where the depth is much greater. Fig. 1*b* also demonstrates the formation of an array-scale wake around the single row of turbines located at $x/d = 0$, and shows that this wake extends beyond the end of the shallow channel and into deeper water.

In the absence of turbines, the flow loses energy to seabed drag, changes in cross-section, and turbulent mixing. The drag due to seabed roughness is calculated as $\mathbf{F} = \rho A_b \mathbf{u}|\mathbf{u}|C_d$, in which ρ is the fluid density, A_b is the plan area of the seabed, $\mathbf{u}$ is the depth-averaged velocity vector, and C_d is a dimensionless seabed drag coefficient. For large-scale tidal models such as these, C_d values of ~ 0.0025 are typical (Soulsby, 1997) but, in this study, a much lower seabed drag coefficient is chosen to ensure that the results from the numerical model are comparable to those of the frictionless two-scale actuator disc theory. A value of C_d = 0.0005 is found by iteration to provide a good compromise between minimising the effects of channel background roughness and maintaining model stability. A relatively small head difference of $\zeta = 0.05$ m, which produces an unexploited channel velocity of $u_0 \approx 0.964$ m/s, is then selected to ensure that the model remains stable even for very high turbine resistance. Mixing is controlled by a spatially and temporally constant horizontal eddy viscosity coefficient, the value of which is calculated, following Borthwick & Barber (1992) and Kuipers & Vreugdenhil (1973), as $\nu = 5.9h|\mathbf{u}|\sqrt{C_d} \approx 2.55\,\mathrm{m}^2/\mathrm{s}$, in which $h = d + \eta$ is the total depth of flow, with d the still water depth and η the free surface elevation.

2.2 Local-scale flow

The extraction of energy and resulting changes to the flow field are simulated using the open channel actuator disc model derived by Houlsby et al. (2008). Following Draper et al. (2010) and Draper (2011), Serhadlıoğlu (2014) introduced this actuator disc model into the DG-ADCIRC code at sub-grid scale, thereby enabling idealised turbines, each defined by a local blockage ratio and local resistance coefficient, to be inserted between numerical elements within the computational grid. The channel-scale flow between these elements

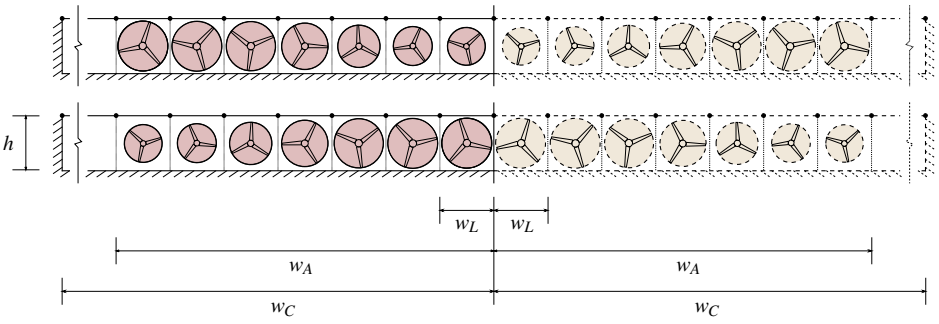

Fig. 2: (Colour online.) Schematic representations (cross-sectional views) of turbine arrays with non-uniform local blockage profiles and their implied reflectional symmetries.

provides boundary conditions for the turbine model within their shared edge, which calculates the extracted power and imposes the associated loss of momentum as a discontinuous reduction in fluid depth (Draper et al., 2010). Coupling the DG-ADCIRC and actuator disc models in this way allows the largely two-dimensional array-scale flow problem to be solved numerically, whilst the highly three-dimensional local-scale problem is modelled analytically at sub-grid scale. Though simplistic, this line sink modelling approach has been shown by laboratory experiment to be a reasonably accurate means of describing the momentum deficit imparted by model-scale rows of porous discs (Draper et al., 2013).

The local blockage ratio is defined, following Nishino & Willden (2012) and Vogel et al. (2016), as $B_L = A_T/hw_L$, in which A_T is the swept area of the turbine, h is the total depth of flow, and w_L is the width of the local flow passage. Assuming a single cross-stream row comprising turbines of equal size and spacing, the global blockage may then be expressed as $B_G = nA_T/hw_C$, in which n is the number of turbines and w_C is the channel width; and the array blockage defined as $B_A = hw_A/hw_C$, in which $w_A(= nw_L)$ is the array width (see Fig. 2). The local resistance is represented, following Houlsby et al. (2008) and Draper et al. (2010), by a local wake velocity coefficient α_{4L}, which is defined as the ratio of the velocity at the pressure equalisation point in the near wake of the turbine to the velocity measured far upstream of the turbine. In this particular code, the local blockage and resistance of the turbine(s) within a given numerical edge are determined by the average of the B_L and α_{4L} values assigned to the two computational nodes which the edge connects (see Fig. 2).

147 The depth and velocity of the flow passing through the turbine(s) are similarly obtained
148 as the averages of the values calculated at these two connected nodes. The actuator disc
149 model allows array performance to be measured using different metrics, three of which are
150 considered in this study: the extractable power P_{ex}, which is defined as the total amount
151 of power removed from the flow; the available power P_{av}, which is defined as the amount
152 remaining when the power dissipated in local-scale mixing is subtracted from P_{ex}; and the
153 global power coefficient C_{PG}, which is defined as the ratio of P_{av} to the kinetic energy flux
154 of channel-scale flow measured just downstream of the channel entrance.

155 ## 2.3 Validation

156 A uniform, unstructured grid is used to discretise the model domain into 17,436 triangular
157 elements, with short sides ranging in length from 100 m in the central channel to 2 km at
158 the ocean boundaries. A single cross-stream row of turbines with global blockage $B_G = 0.1$
159 is then extended inward from one side of the channel, and a steady current is produced by
160 establishing a fixed head difference of $\zeta = 0.05$ m between the upstream and downstream
161 ocean boundaries. Linear basis functions are specified and the model solutions are advanced
162 in time using a second-order Runge-Kutta scheme with a 1 s time step. The model is allowed
163 to spin up from still water conditions for 2 days, after which results from the following 12
164 hours are extracted and time-averaged. In this steady, low roughness flow, a high turbine
165 resistance produces a gently undulating array-scale wake, broadly similar to that which may
166 be observed behind a bluff body at subcritical Reynolds number. The effect of this unsteadi-
167 ness is to extend greatly the amount of time required for the model to achieve a (near) steady
168 state and thus ensure that the chosen sampling period overestimates the performance of high
169 resistance arrays. Whilst this problem is thought not to affect the overall conclusions of the
170 present work, the effect of unsteady wakes on power production will clearly require further
171 investigation with a more sophisticated numerical model.

172 Despite key differences in the underlying assumptions, the numerical array and channel
173 models are shown to reproduce quite well the predictions from the corresponding theoretical
174 models. Estimates of the channel's maximum extractable power (also known as the channel's

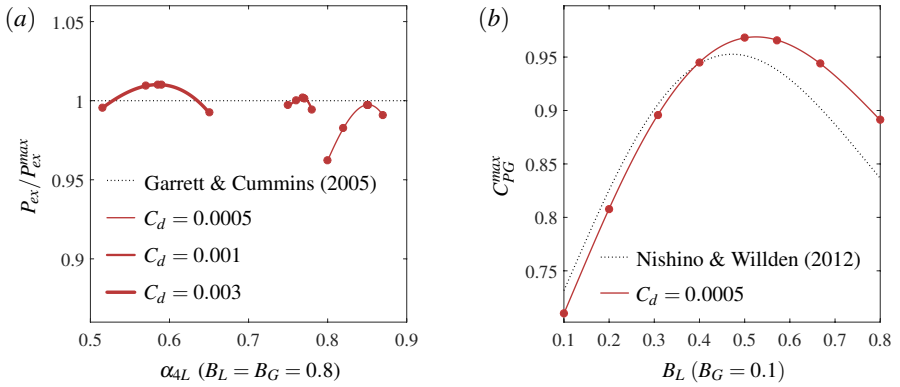

Fig. 3: (Colour online.) Comparisons between numerical (solid lines) and theoretical (dotted lines) model results for uniform arrays in channels with seabed drag coefficient C_d and flow driven by head difference $\zeta = 0.0025d$: (a) estimates of maximum extractable power P_{ex}^{max} for very large, full-width arrays, and; (b) variation in maximum global power coefficient C_{PG}^{max} with local blockage B_L for the chosen array.

'potential'), calculated for different seabed drag coefficients and using very large, full-width arrays ($B_L = B_G = 0.8$), are found to match with predictions from the theoretical channel model of Garrett & Cummins (2005) (Fig. 3a); whilst the measured variation in maximum global power coefficient with local blockage is found to agree well with results from the two-scale actuator disc theory of Nishino & Willden (2012) (Fig. 3b). The agreement with two-scale theory is shown to be poorer at high local blockage where the model is known to overestimate the performance of the array, but clearly sufficient to capture the leading-order physics.

3 Results

Optimal uniform turbine arrangements are first identified by interpolating between uniform local blockage B_L and local resistance α_{4L} profiles. The following near-optimal uniform arrangements (to the nearest whole number of turbine edges) are then chosen as the starting points for the analysis: $B_L = 0.5714$ and $\alpha_{4L} = 0.583$, which produce a global power coefficient C_{PG} of $\sim$0.966; and $B_L = 0.2$ and $\alpha_{4L} = 0.424$, which yield an available power P_{av} of $\sim$2.311 MW, or $\sim$ 16% of the channel's $\sim$14.6 MW potential. The arrangements which maximise P_{av} and C_{PG} are quite different, in this case, because the low background rough-

ness makes the channel-scale kinetic energy flux quite sensitive to the turbine resistance (Bonar, 2017).

Starting with these near-optimal uniform arrangements, the effects of non-uniformity on array performance are explored by varying B_L and α_{4L} across the width of the array. The resulting non-uniform profiles are considered bilaterally symmetric due to their reflectional symmetry about the mainland boundary from which the array is extended into the channel (see Figs. 1 and 2), and include arrays with uniform B_L but non-uniform α_{4L}, uniform α_{4L} but non-uniform B_L, and select examples for which both B_L and α_{4L} are non-uniform. In all cases B_L and α_{4L} are varied linearly across the turbine edges, with variations denoted by the extreme values at the edges nearest to (centre edge) and furthest from (end edge) the channel wall (see Fig. 2). In addition to C_{PG} and P_{av}, the effects of non-uniform local blockage and resistance on the local-scale extraction efficiency, which is defined as the ratio of P_{av} to P_{ex}, and channel-scale kinetic energy flux are also considered. For brevity, however, the corresponding figures for these additional metrics are placed in an appendix.

3.1 Non-uniform local resistance

The analysis begins by exploring the performance of arrays with uniform local blockage B_L but non-uniform local resistance α_{4L}. Figs. 4*a* and 4*b* illustrate the variations in global power coefficient C_{PG} and available power P_{av} with centre and end local resistance α_{4L}, normalised by the values obtained using the initial uniform arrangements.

Although the values of C_{PG} obtained using non-uniform α_{4L} are not quite as high as that obtained using uniform α_{4L}, Fig. 4*a* shows that a considerable range of non-uniform local resistance profiles produce global power coefficients within $\sim$3% of this value. Fig. 4*b* reveals a similar trend for P_{av}, for which the corresponding range is even greater. (The corresponding variations in local-scale extraction efficiency and channel-scale kinetic energy flux are shown in the appendix — see Figs. A1 and A2.) These findings agree with those of Adcock (2015), who used a similar DG-ADCIRC model to show that although linear variations in local resistance can produce up to 5% more power in horizontally sheared flow, the performance of the array is relatively insensitive to the local resistance profile.

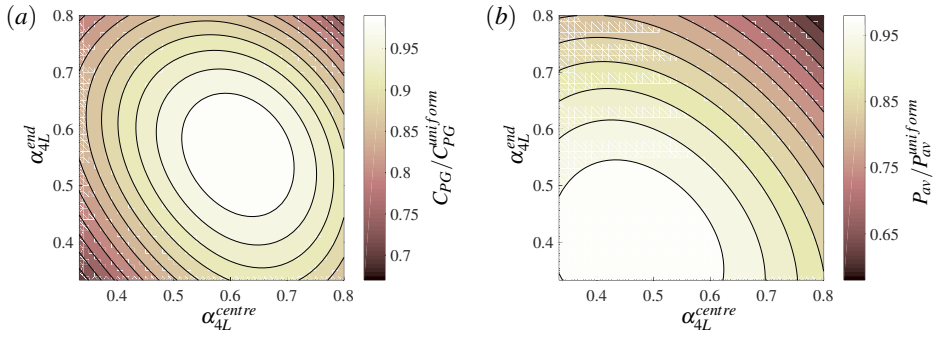

Fig. 4: (Colour online.) Variation in normalised: (a) global power coefficient C_{PG}, and; (b) available power P_{av}; with centre and end local resistance α_{4L}^{centre} and α_{4L}^{end} for arrays of near-optimal uniform local blockage.

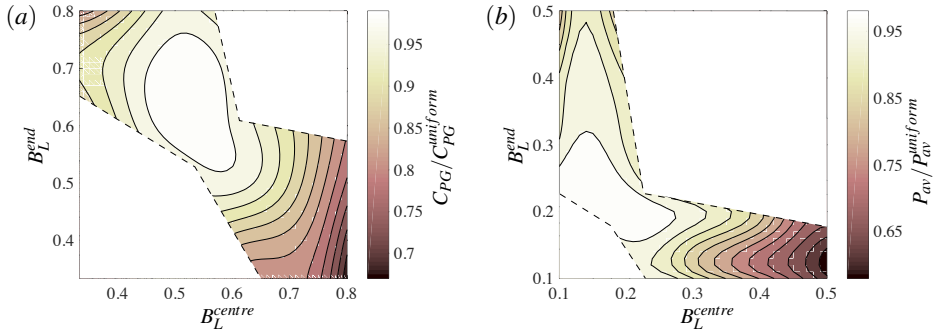

Fig. 5: (Colour online.) Variation in normalised: (a) global power coefficient C_{PG}, and; (b) available power P_{av}; with centre and end local blockage B_L^{centre} and B_L^{end} for arrays of near-optimal uniform local resistance.

3.2 Non-uniform local blockage

Arrays with uniform local resistance α_{4L} but non-uniform local blockage B_L are considered next. Figs. 5*a* and 5*b* illustrate the variations in global power coefficient C_{PG} and available power P_{av} with centre and end local blockage B_L, normalised by the values obtained using the initial uniform arrangements. (Figs. A3 and A4 show the corresponding variations in local-scale extraction efficiency and channel-scale kinetic energy flux.) The solution space is reduced in this case because the variation in B_L is subject to the additional constraint that the global blockage ratio B_G must always equal 0.1.

Fig. 5*a* shows that, as with non-uniform α_{4L}, there is a significant range of non-uniform B_L profiles which produce C_{PG} values quite close to that of the uniform arrangement. Fig. 5*b* reveals that the trend for P_{av} is again similar to that for C_{PG}, and that for both metrics,

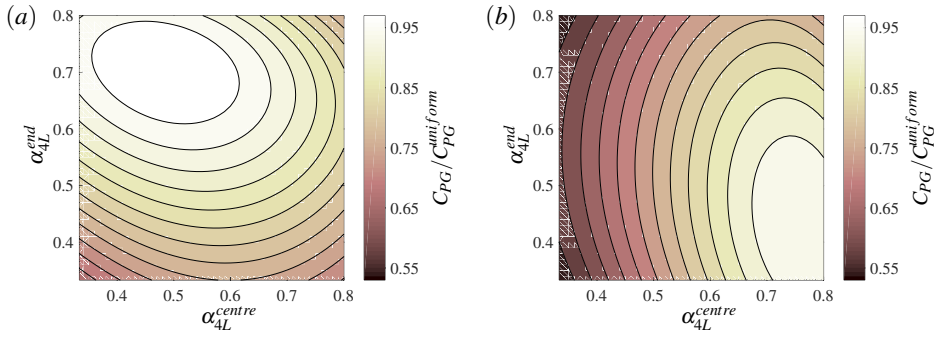

Fig. 6: (Colour online.) Variation in normalised global power coefficient C_{PG} with centre and end local resistance α_{4L}^{centre} and α_{4L}^{end} for arrays with: (a) higher local blockage at their ends ($B_L^{end} = 0.7$) than at their centre ($B_L^{centre} = 0.4$), and; (b) higher local blockage at their centre ($B_L^{centre} = 0.7$) than at their ends ($B_L^{end} = 0.4$).

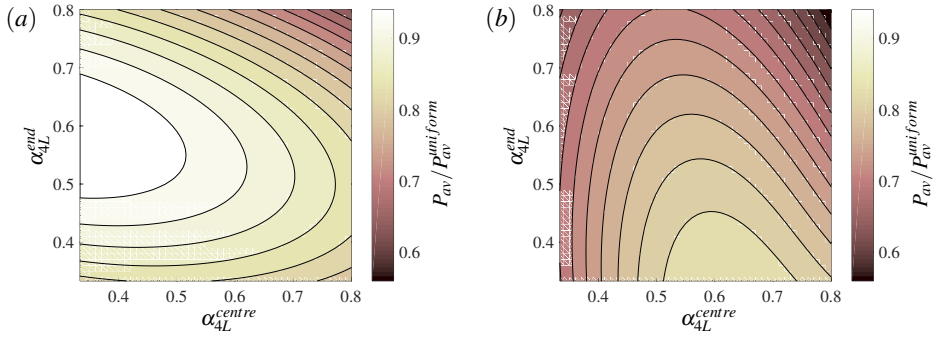

Fig. 7: (Colour online.) Variation in normalised available power P_{av} with centre and end local resistance α_{4L}^{centre} and α_{4L}^{end} for arrays with: (a) higher local blockage at their ends ($B_L^{end} = 0.4$) than at their centre ($B_L^{centre} = 0.1$), and; (b) higher local blockage at their centre ($B_L^{centre} = 0.4$) than at their ends ($B_L^{end} = 0.1$).

there is clear advantage to placing the larger turbines (i.e. those with higher values of B_L) on the ends of the array rather than in the centre.

3.3 Non-uniform local blockage and resistance

Lastly, four examples of arrays with both non-uniform local blockage B_L and non-uniform local resistance α_{4L} are considered. Figs. 6 and 7 illustrate the variations in normalised global power coefficient C_{PG} and normalised available power P_{av} with centre and end local resistance α_{4L} for arrays with higher local blockage B_L at their ends than at their centre, and for arrays with higher B_L at their centre than at their ends. (Figs. A5, A6, A7, and A8 show the corresponding variations in local-scale extraction efficiency and channel-scale kinetic

energy flux.) The selected local blockage profiles vary from $B_L = 0.4$ to $B_L = 0.7$ for C_{PG} and from $B_L = 0.1$ to $B_L = 0.4$ for P_{av}.

Figs. 6 and 7 clearly demonstrate that the performance of the uniform arrays cannot be exceeded, or even matched, by varying both B_L and α_{4L} together across the width. These figures also show that arrays with larger turbines at their ends consistently outperform those with larger turbines at their centre. The peak normalised C_{PG} for the array with higher B_L at its ends is not only higher than that of the array with higher B_L at its centre ($\sim$0.99 vs. $\sim$0.96), but is achieved with less variation in α_{4L} across the width ($\sim 0.48 \leq \alpha_{4L} \leq \sim 0.71$ vs. $\sim 0.44 \leq \alpha_{4L} \leq \sim 0.76$), a higher normalised channel-scale kinetic energy flux ($\sim$1.14 vs. $\sim$1.01 — see Fig. A6), and only slightly lower normalised local-scale extraction efficiency ($\sim$1.02 vs. $\sim$1.04 — see Fig. A5). The results for P_{av} are again similar: the array with larger turbines at its ends produces a higher peak normalised P_{av} ($\sim$0.96 vs. $\sim$0.85), with less spanwise variation in α_{4L} ($\sim 0.33 \leq \alpha_{4L} \leq \sim 0.58$ vs. $\sim 0.33 \leq \alpha_{4L} \leq \sim 0.62$), a higher channel-scale kinetic energy flux ($\sim$0.96 vs. $\sim$0.86 — see Fig. A8), and only slightly lower local-scale efficiency ($\sim$1.08 vs. $\sim$1.11 — see Fig. A7). It is also worth noting that for all non-uniform arrays considered, power performance is maximised by tuning the smaller turbines (i.e. those with lower values of B_L) to present higher local resistances (i.e. lower values of α_{4L}) than the larger turbines.

4 Discussion

Given that turbine performance is a function of both blockage and resistance, it is unsurprising that the performance of a turbine array in an initially uniform flow field cannot be improved by varying solely the local blockage B_L or solely the local resistance α_{4L} across the width. For a given B_L, there exists a unique α_{4L} to maximise either the available power P_{av} or average global power coefficient C_{PG}. It seems intuitive, then, that varying B_L and α_{4L} independently of each other simply results in sub-optimal performance for the vast majority of turbines within the array. This finding agrees with Hunter et al. (2015), who used three-dimensional Reynolds-averaged Navier-Stokes simulations of porous discs to show that the average global power coefficient C_{PG} for a cross-stream row of uniform B_L is maximised

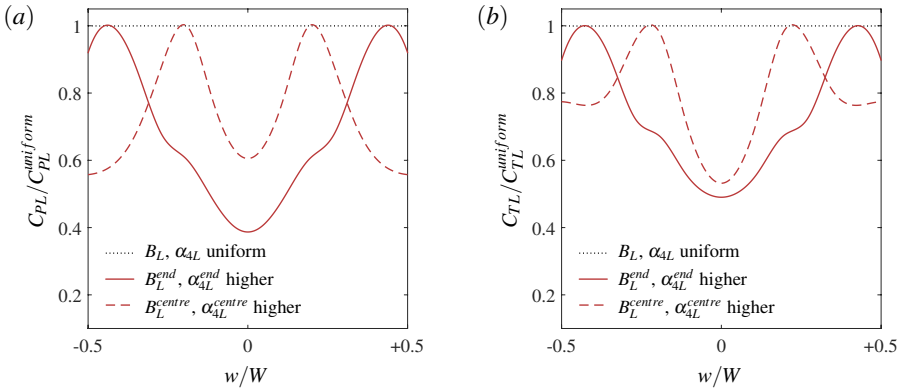

Fig. 8: (Colour online.) Variation in normalised: (a) local power coefficient C_{PL}, and; (b) local thrust coefficient C_{TL}; across the array width W for near-optimally tuned uniform and non-uniform arrays.

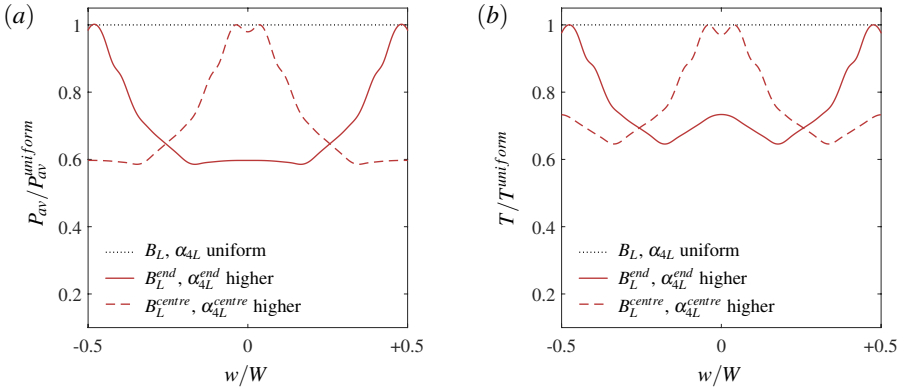

Fig. 9: (Colour online.) Variation in normalised: (a) available power P_{av}, and; (b) applied thrust T; across the array width W for near-optimally tuned uniform and non-uniform arrays.

by a uniform α_{4L}. The finding does not agree, however, with Cooke et al. (2016), who used a three-scale actuator disc model to show that a cross-stream row with uniform α_{4L} but non-uniform B_L can produce a higher peak C_{PG} than can be produced using the two-scale actuator disc model of Nishino & Willden (2012), for which both B_L and α_{4L} are uniform. That being said, it should also be noted that the third scale of mixing introduced by Cooke et al. (2016) divides the single row of turbines into multiple sub-rows within the same plane, thereby creating non-uniform B_L profiles much more complicated than the simple linear variations considered here.

Interestingly, it appears that neither can array performance be improved by varying both B_L and α_{4L} together across the array width. Figs. 8 and 9 show that although certain non-

uniform configurations can produce similar values of C_{PG} or P_{av} to those of the uniform arrays, the operation of these non-uniform arrays is fundamentally different at local-scale, requiring large variations in both power and thrust among the turbines, which are undesirable from a design perspective.

For all non-uniform arrays considered, the optimum strategy appears to be to tune the smaller turbines to present higher local resistances than the larger turbines. This does not appear to be a means by which to compensate for the variation in local blockage across the array width because it is not the most uniform variations in thrust and power which produce peak array performance. Rather, it implies there is some advantage in tuning the smaller turbines, which produce the least power, sub-optimally in order to divert more flow into the path of the larger turbines which produce the most power. This would also explain why it appears to be better to place the smaller, more resistant turbines at the centre of the array rather than at its ends — because placing the smaller, more resistant turbines at the centre ensures that there are larger turbines either side to take full advantage of the flow which is diverted both left and right.

5 Conclusions

Simple theoretical models have provided a number of valuable insights to inform the design of tidal turbine arrays, but have only recently begun to account for the non-uniformity inherent in the flow conditions that tidal turbines experience. The work of Draper et al. (2016), which extends the classical actuator disc model to incorporate an inviscid shear flow, represents a considerable advance toward this goal. To investigate the effects of sheared flow, Draper et al. (2016) analyse the performance of an idealised turbine represented by a uniform local resistance in a non-uniform flow field. Draper et al. (2016) also note, however, that their analysis could be extended to incorporate non-uniform local resistances in order to provide a better approximation of a tidal turbine array.

In this paper, we take the first step toward such an extension by using depth-averaged numerical simulations to investigate the performance of non-uniform tidal turbine arrays in uniform flow. Results from the combined array and channel model of Bonar (2017) sug-

gest that the performance of a tidal turbine array in an initially uniform flow field cannot be improved by varying solely the local blockage, solely the local resistance, or both local blockage and resistance together, across the array width. Certain non-uniform configurations are found to produce similar power outputs and global power coefficients to those of uniform arrays, but the operation of these non-uniform arrays is shown to require large and undesirable variations in thrust and power among the turbines. These results suggest that for an initially uniform flow field, the optimal tidal turbine array is also uniform, that is to say that it comprises turbines of equal size, spacing, and resistance. This finding is encouraging because it is more cost-effective and much simpler to design each turbine to be the same and to operate in the same way. The result is also somewhat intuitive and, together with the findings of Adcock (2015) and Draper et al. (2016) on the performance of turbines in horizontally and vertically sheared flows, suggests a more general, and perhaps unsurprising, conclusion that tidal turbine arrays perform best when designed to account specifically for the flow conditions that they are to experience.

Finally, we note that our analysis can, of course, be extended in many different ways. The present model can be adapted, for instance, to explore the effects of varying both local blockage and resistance in non-uniform flow fields, or to incorporate channel-scale dynamics and time-variable turbine tuning strategies (e.g. Vennell & Adcock, 2014; Vennell, 2016). A more thorough analysis will, however, require a more sophisticated numerical model to describe more accurately the individual and collective interactions with the flow which define the performance of tidal turbines in arrays.

Acknowledgements This paper is based on part of the first author's PhD studies, which were supported by the Energy Technology Partnership and Scotland's Saltire Prize Challenge competitors: Aquamarine Power, MeyGen Ltd, Pelamis Wave Power, ScottishPower Renewables, and West Islay Tidal Energy Park Ltd, under Scottish Government Grant R43039 (Saltire Studentship). The authors wish to thank Prof. Matthew Piggott, Prof. Paolo Perona, and three anonymous reviewers for providing valuable feedback on this work.

331 ## Appendix

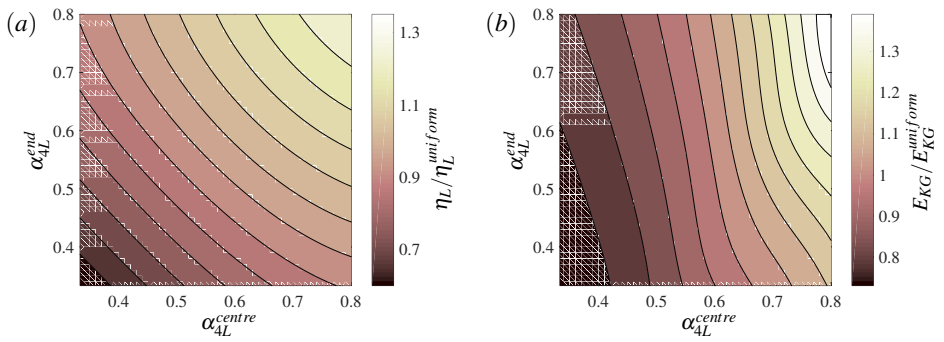

Fig. A1: (Colour online.) Variation in normalised: (a) local-scale extraction efficiency η_L, and; (b) channel-scale kinetic energy flux E_{KG}; corresponding to Fig. 4*a*.

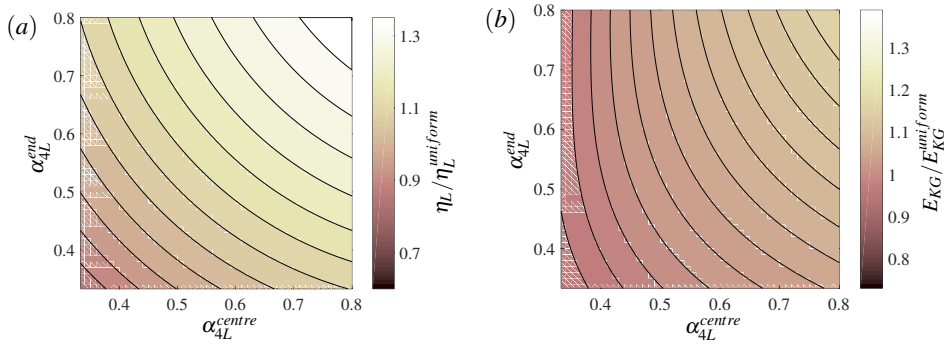

Fig. A2: (Colour online.) Variation in normalised: (a) local-scale extraction efficiency η_L, and; (b) channel-scale kinetic energy flux E_{KG}; corresponding to Fig. 4*b*.

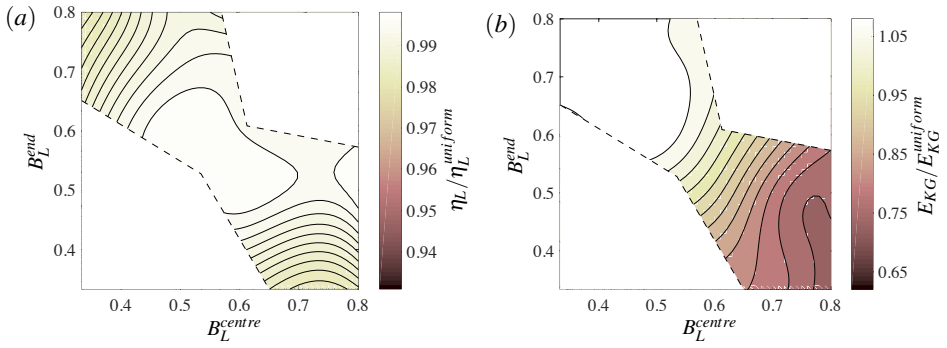

Fig. A3: (Colour online.) Variation in normalised: (a) local-scale extraction efficiency η_L, and; (b) channel-scale kinetic energy flux E_{KG}; corresponding to Fig. 5*a*.

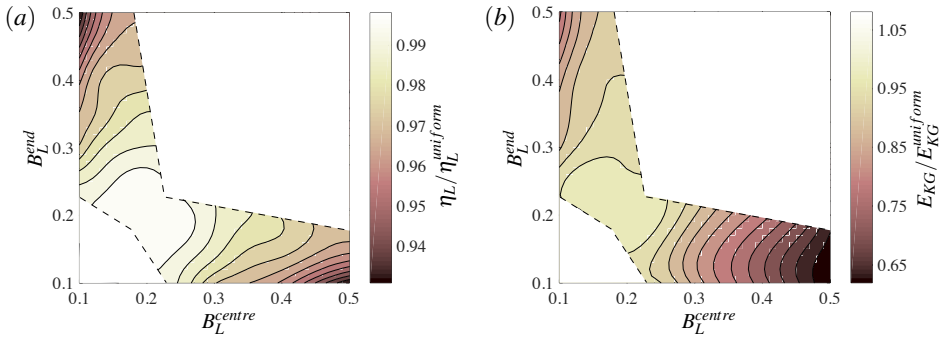

Fig. A4: (Colour online.) Variation in normalised: (a) local-scale extraction efficiency η_L, and; (b) channel-scale kinetic energy flux E_{KG}; corresponding to Fig. 5*b*.

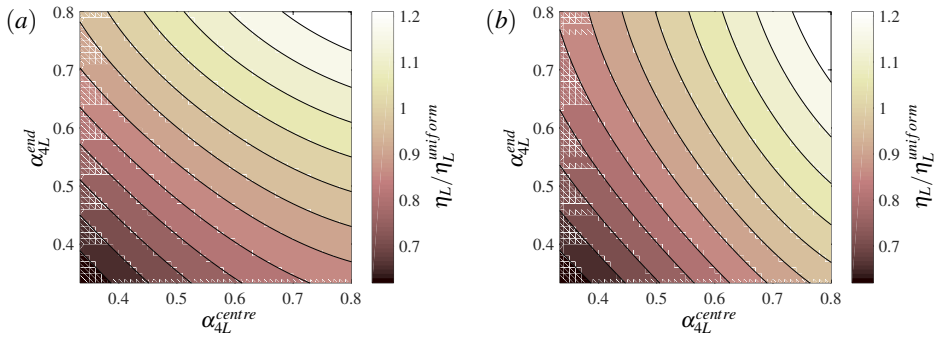

Fig. A5: (Colour online.) Variation in normalised local-scale extraction efficiency η_L corresponding to: (a) Fig. 6*a*, and; (b) Fig. 6*b*.

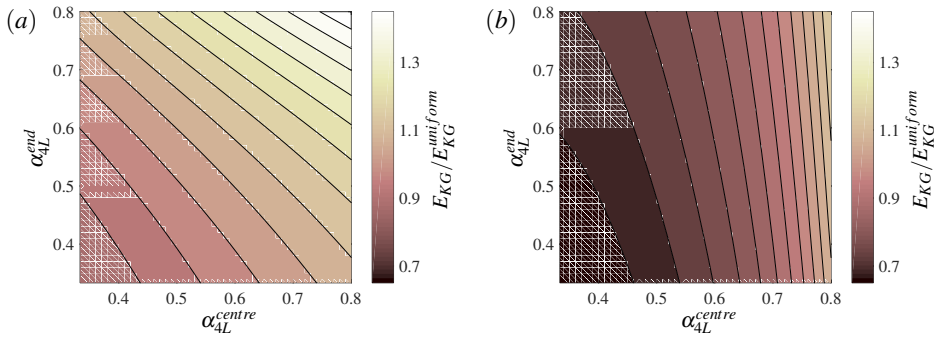

Fig. A6: (Colour online.) Variation in normalised channel-scale kinetic energy flux E_{KG} corresponding to: (*a*) Fig. 6*a*, and; (*b*) Fig. 6*b*.

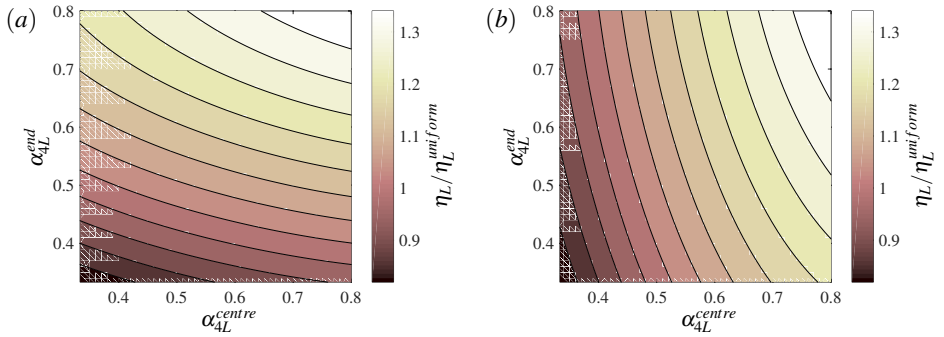

Fig. A7: (Colour online.) Variation in normalised local-scale extraction efficiency η_L corresponding to: (*a*) Fig. 7*a*, and; (*b*) Fig. 7*b*.

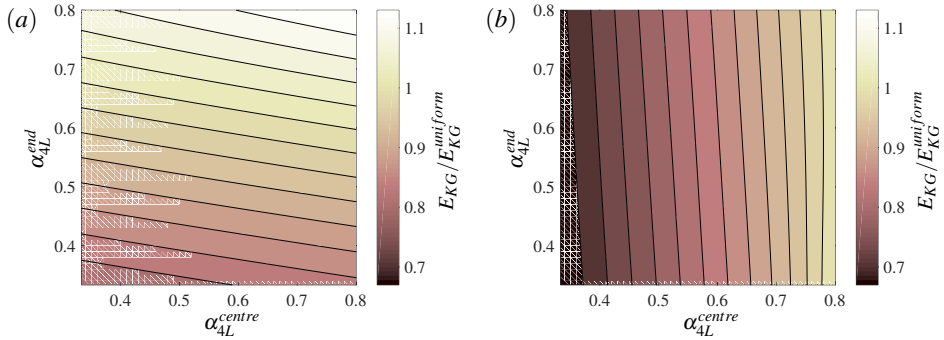

Fig. A8: (Colour online.) Variation in normalised channel-scale kinetic energy flux E_{KG} corresponding to: (*a*) Fig. 7*a*, and; (*b*) Fig. 7*b*.

References

Adcock, TAA, Borthwick, AGL, Houlsby, GT (2011) The open boundary problem in tidal basin modelling with energy extraction. Proceedings of the 9th European Wave and Tidal Energy Conference, Southampton, UK.

Adcock, TAA, Draper, S, Nishino, T (2015) Tidal power generation – A review of hydrodynamic modelling. Proc Inst Mech Eng A 229(7):755–771, https://doi.org/10.1177/0957650915570349.

Adcock, TAA (2015) On tidal stream turbines placed off headlands. J Renew Sustain Energy 7(6):061706, https://doi.org/10.1063/1.4936361.

Betz, A (1920) Das Maximum der Theoretisch Möglichen Ausnützung des Windes durch Windmotoren. Z. Gesamte Turbinenwesen 26(307–309), pp 8.

Bonar, PAJ (2017) Toward best practice in the design of tidal turbine arrays. PhD Thesis, University of Edinburgh, UK.

Borthwick, AGL, Barber, RW (1992) River and reservoir flow modelling using the transformed shallow water equations. Int J Numer Meth Fl 14(10):1193–1217, https://doi.org/10.1002/fld.1650141005.

Burton, T, Sharpe, D, Jenkins, N, Bossanyi, E (2001) Wind energy handbook. John Wiley & Sons, Ltd.

Cooke, SC, Willden, RHJ, Byrne, BW (2016) The potential of cross-stream aligned sub-arrays to increase tidal turbine efficiency. Renew Energy 97:284–292, https://doi.org/10.1016/j.renene.2016.05.087.

Draper, S, Houlsby, GT, Oldfield, MLG, Borthwick, AGL (2010) Modelling tidal energy extraction in a depth-averaged coastal domain. IET Renew Pow Gener 4(6):545–554, https://doi.org/10.1049/iet-rpg.2009.0196.

Draper, S (2011) Tidal stream energy extraction in coastal basins. DPhil Thesis, University of Oxford, UK.

Draper, S, Stallard, T, Stansby, P, Way, S, Adcock, T (2013) Laboratory scale experiments and preliminary modelling to investigate basin scale tidal stream energy extraction. Proceedings of the 10th European Wave and Tidal Energy Conference, Aalborg, Denmark.

Draper, S, Nishino, T (2014a) Centred and staggered arrangements of tidal turbines. J Fluid Mech 739:72–93, https://doi.org/10.1017/jfm.2013.593.

Draper, S, Nishino, T (2014b) Centred and staggered arrangements of tidal turbines – ERRATUM. J Fluid Mech 743:636, https://doi.org/10.1017/jfm.2014.53.

Draper, S, Nishino, T, Adcock, TAA, Taylor, PH (2016) Performance of an ideal turbine in an inviscid shear flow. J Fluid Mech 796:86–112, https://doi.org/10.1017/jfm.2016.247.

Garrett, C, Cummins, P (2005) The power potential of tidal currents in channels. Proc R Soc A 461(2060):2563–2572, https://doi.org/10.1098/rspa.2005.1494.

Garrett, C, Cummins, P (2007) The efficiency of a turbine in a tidal channel. J Fluid Mech 588:243–251, https://doi.org/10.1017/S0022112007007781.

Garrett, C, Greenberg, D (1977) Predicting changes in tidal regime: The open boundary problem. J Phys Oceanogr 7(2):171–181, doi:10.1175/1520-0485(1977)007<0171:PCITRT>2.0.CO;2.

Houlsby, GT, Draper, S, Oldfield, MLG (2008) Application of linear momentum actuator disc theory to open channel flow. Tech Rep OUEL 2296/08, Department of Engineering Science, University of Oxford, UK.

Hunter, W, Nishino, T, Willden, RHJ (2015) Investigation of tidal turbine array tuning using 3D Reynolds-averaged Navier-Stokes simulations. Int J Mar Energy 10:39–51, https://doi.org/10.1016/j.ijome.2015.01.002.

Joukowsky, NE (1920) Windmill of the NEJ type. Trans Cent Inst Aero-Hydrodyn Moscow, pp 57.

Kubatko, EJ, Westerink, JJ, Dawson, C (2006) hp discontinuous Galerkin methods for advection dominated problems in shallow water flow. Comput Method Appl Mech Engrg 196(1–3):437–451, https://doi.org/10.1016/j.cma.2006.05.002.

Kubatko, EJ, Bunya, S, Dawson, C, Westerink, JJ, Mirabito, C (2009) A performance comparison of continuous and discontinuous finite element shallow water models. J Sci Comput 40(1–3):315–339, https://doi.org/10.1007/s10915-009-9268-2.

Kuipers, J, Vreugdenhil, CB (1973) Calculations of two-dimensional horizontal flow. Res Rep S163 Pt. 1, Delft Hydraulics Laboratory, The Netherlands.

Nishino, T, Willden, RHJ (2012) The efficiency of an array of tidal turbines partially blocking a wide channel. J Fluid Mech 708:596–606, https://doi.org/10.1017/jfm.2012.349.

Nishino, T, Willden, RHJ (2013) Two-scale dynamics of flow past a partial cross-stream array of tidal turbines. J Fluid Mech 730:220–244, https://doi.org/10.1017/jfm.2013.340.

Okulov, VL, van Kuik, GAM (2012) The Betz–Joukowsky limit: On the contribution to rotor aerodynamics by the British, German, and Russian scientific schools. Wind Energy 15(2):335–344, https://doi.org/10.1002/we.464.

Serhadlıoğlu, S (2014) Tidal stream resource assessment of the Anglesey Skerries and the Bristol Channel. DPhil Thesis, University of Oxford, UK.

Soulsby, RL (1997) Dynamics of marine sands: A manual for practical applications. Telford, London.

Whelan, JI, Graham, JMR, Peiró, J (2009) A free-surface and blockage correction for tidal turbines, J Fluid Mech 624:281–291, https://doi.org/10.1017/S0022112009005916.

Vennell, R (2010) Tuning turbines in a tidal channel, J Fluid Mech 663:253–267, doi:10.1017/S0022112010003502.

Vennell, R, Adcock, TAA (2014) Energy storage inherent in large tidal turbine farms, Proc R Soc A 470(2166):20130580, doi:10.1098/rspa.2013.0580.

Vennell, R, Funke, SW, Draper, S, Stevens, C, Divett, T (2015) Designing large arrays of tidal turbines: A synthesis and review, Renew Sust Energy Rev 41:454–472, doi:10.1016/j.rser.2014.08.022.

Vennell, R (2016) An optimal tuning strategy for tidal turbines, Proc R Soc A 472(2195):20160047, doi:10.1098/rspa.2016.0047.

Vogel, CR, Houlsby, GT, Willden, RHJ (2016) Effect of free surface deformation on the extractable power of a finite width turbine array, Renew Energy 88:317–324, https://doi.org/10.1016/j.renene.2015.11.050.

Vogel, CR, Willden, RHJ, Houlsby, GT (2017) Power available from a depth-averaged simulation of a tidal turbine array, Renew Energy 114:513–524, https://doi.org/10.1016/j.renene.2017.07.051.